University of Reading

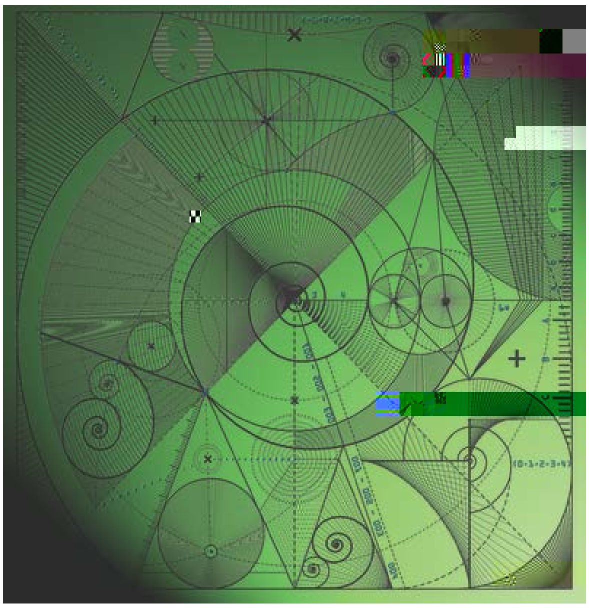

Approximation or SIA (Hutter, 1983). It gives an analytical formulation for horizontal velocities of ice in the sheet and for their vertically averaged counterpart. Although simple and fast, the SIA captures well the nonlinearity of the system and is an excellent resource for testing numerical approaches, since moving-margin exact solutions exist in the literature (Halfar, 1981, 1983; Bueler et al., 2005).

Signi cant e orts have been invested in ice sheet modelling. These have led ice sheet modellers to compare results obtained by various models for the same idealistic test problems (see the EISMINT intercomparison project (Huybrechts et al., 1996; Payne et al., 2000) for ice sheet models using SIA). Most numerical ice sheet simulations use a xed grid to calculate the solution of the ice ow equations. In xed grid models the ice sheet margins are not precisely located as they generally fall between grid points. So in order to obtain a good approximation a high grid resolution is required around the positions of the ice sheet margin during its evolution, which makes xed grid models costly for accurately computing the evolution of the ice margin.

One approach to gain high resolution is to apply adaptative grid techniques, which allow
improveda(e)-3m400(allo)28(w)]TJ 91(app8(ebs)-1((for)8(hes)-1(ie)-1(lo)-27f)1(a(eiw)]TJ 9)-1(s)-334y)]TJ 90

2 Ice sheet modelling

2.1 Ice sheet geometry and Shallow Ice Approximation

We consider a single solid phase ice sheet whose thickness at position $(x; y)$ and time t is denoted by $h(t; x; y)$. We assume that the ice sheet lies on a fixed bedrock and denote by $b(x; y)$ the bed elevation. The surface elevation, $s(t; x; y)$, is then obtained as

$$s = b + h \tag{1}$$

The evolution of ice sheet thickness is governed by the balance between ice gained or lost on the surface, snow precipitation and surface melting, and ice flow draining ice accumulated in the interior towards the edges of the ice sheet. This is summarised in the mass balance equation

$$\frac{\partial h}{\partial t} = m - \nabla \cdot (hU) \quad \text{in} \quad \Omega(t) \tag{2}$$

where $m(t; x; y)$ is the surface mass balance (positive for accumulation, negative for ablation), $U(t; x; y)$ is the vector containing the vertically averaged horizontal components of the velocity of the ice, and $\Omega(t)$ is the area where the ice sheet is located.

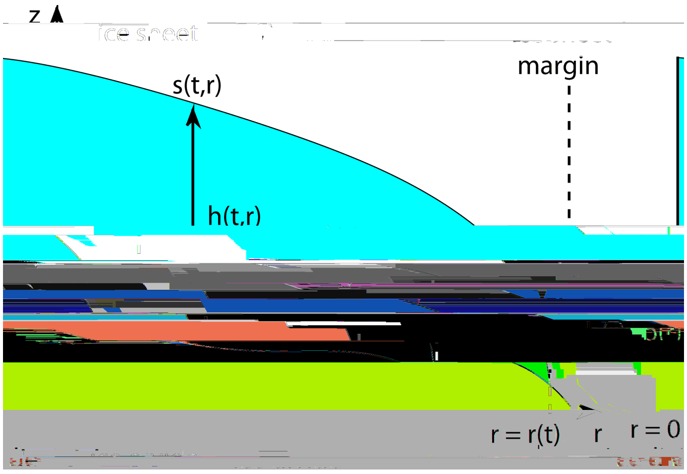

Figure 1: Section of a grounded radially-symmetrical ice sheet.

where $\hat{r}$ is the unit radial vector, and the mass balance Eq. (2) simplifies to

$$\frac{\partial h}{\partial t}$$

2005, 2011; Scherer and Baines, 2012; Lee et al., 2015). This conservation method has been applied in various contexts and is perfectly suitable for multi-dimensional problems (different examples are summarised in Baines et al. (2011) and references therein; see also Partridge (2013) for the special case of ice sheet dynamics). The key points of the method are given in the next paragraphs and the numerical validation of the method is carried out in Sect. 4.

3.1 Conservation of mass fraction

Moving point velocities are derived from the conservation of mass fractions (CMF). To apply this principle we first define the total mass of the ice sheet (t) as

$$(t) = 2 \int_0^{r_l(t)} r\, h(t;r)\, dr \qquad (9)$$

In fact (t) is the total volume of the ice sheet but, since the density of ice is assumed constant everywhere, (t) is proportional to the total mass of the ice sheet and the constant of proportionality cancels out.

Since the flux of ice through the ice sheet margin is assumed to be zero, any change in the total mass over the whole ice sheet is due solely to the surface mass balance $m(t;r)$, and hence the rate of change of the total mass, $\dot{}$, is given by

$$\dot{}(t) = 2 \int_0^{r_l(t)} r\, m(t;r)\, dr \qquad (10)$$

We now introduce the principle of the conservation of mass fractions. Let $\hat{r}(t)$ be a moving point and define $(\hat{r})$ to be the relative mass in the moving subinterval $(0, \hat{r}(t))$ as

$$(\hat{r}) = \frac{2}{(t)} \int_0^{\hat{r}(t)} r\, h(t;r)\, dr \qquad (11)$$

The rate of change of $\hat{r}(t)$ is determined by keeping $(\hat{r})$ independent of time for all moving subdomains of $[0, r_l(t)]$. Note that $(\hat{r}) \in [0;1]$ is a cumulative function with $(0) = 0$ and $(r_l) = 1$.

3.2 Trajectories

The point at r

close to the boundary $(r_l(t) - \hat{r}(t))^{\alpha(t)+1} g_l(t)$ is constant in time. Hence, since $(r_l(t) - \hat{r}(t))$ is decreasing, $\alpha(t)$ is also decreasing. When $\alpha(t)$ reaches $n/(2n+1)$ the boundary moves.

It is a technical exercise to show that this property extends to cases with accumulation/ablation and with a general bedrock with a finite slope $\partial b/\partial r$ at the margin (see Partridge, 2013). The key point to notice is that the asymptotic behaviour depends on an infinite slope of h at the margin whereas $b(r)$ always has a finite slope.

3.5 Numerics

We now implement a numerical scheme using a finite difference method. The complete algorithm is detailed in Appendix B. In addition, we explain in Appendix B.6 why our implementation respects the asymptotic behaviour of the ice sheet at its margin.

4 Numerical results

This section is dedicated to the validation of the numerical scheme derived from the moving point method detailed in Sect. 3 and to the study of its behaviour. Every numerical experiment is performed with the parameter values given in Table 1.

4.1 Steady states with flat bedrock

We start by studying the behaviour of the numerical scheme using a surface mass balance $m(r)$ constant in time in order to define a steady state. When the steady state is reached, from Eq. (5), the following relationship is valid:

$$r m = \frac{\partial}{\partial r}\left(r h^{1} \ldots\right.$$

As a first test, we consider initialising our numerical model with the following profile:

$$h(t_0; r) = h_0 \left(1 - \left(\frac{r}{r_l(t_0)} \right)^2 \right)^p \tag{23}$$

and study the convergence towards the steady state in three different cases. In each experiment, the initial grid has 21 points and the model is run for 10 000 a with a constant time step $\Delta t = 0.1$ a. We now detail the initial state for each experiment:

a. Uniformly distributed initial grid with $r_l(0) = 450$ km, $h_0 = 1000$ m and $p = 3/7$.

b. Initial grid with $r_l(0) = 500$ km with higher resolution near the margin, $h_0 = 1000$ m and $p = 1$.

c. Uniformly distributed initial grid with $r_l(0) = 600$ km, $h_0 = 4000$ m and $p = 1/4$.

The evolution of the geometry and the overall motion of the grid points are shown for each experiment in Fig. 2. The three experiments show the convergence of every initial state towards the same steady state. These experiments also show the ability of the CMF method to capture the trajectory of the moving ice sheet margin (in advance and retreat).

Figure 2: Evolution of the geometry and overall motion of the grid points for three experiments with the EISMINT surface mass balance and initial profile described by Eq. (23). Top: initial uniform grid with $r_l(0) = 450$ km, $h_0 = 1000$ m and $p = 3/7$, middle: initial grid with higher resolution near the margin with $r_l(0) = 500$ km, $h_0 = 1000$ m and $p = 1$, bottom: initial uniform grid with $r_l(0) = 600$ km, $h_0 = 4000$ m and $p = 1/4$.

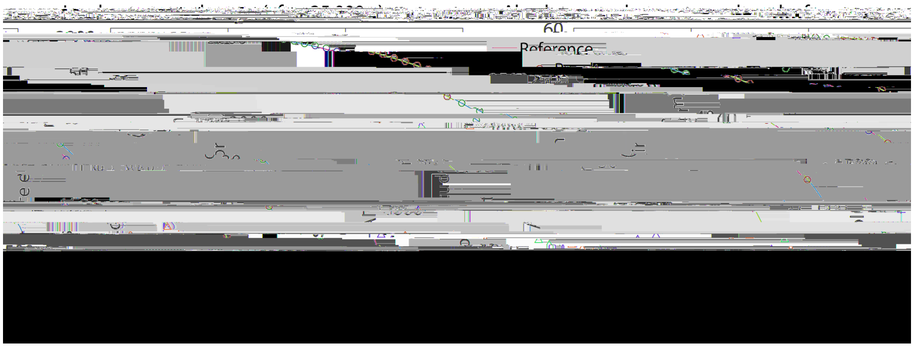

Figure 3: The steady state from the EISMINT moving-margin experiment compared with our 25 000 a model run with 28 nodes, uniformly distributed at the initial time. The reference profile is obtained by a numerical integration of Eq. (21) using a composite trapezoidal rule. The error in the ice thickness occurs mostly near the ice sheet margin, as in other experiments (RMS error is 15.71 m and maximum error is 58.23 m). The position of the margin is well determined as the absolute error is only 138.5 m.

We now perform the moving-margin EISMINT experiment (Huybrechts et al., 1996) in order to validate our numerical model in this case. At the initial time $t = 0$ we prescribe a uniformly distributed grid with $r_l(0) = 450$ km and an initial ice thickness $h(0, r)$ taken as $\Delta t \; \dot{m}(r)$ for the constant time step $\Delta t = 0.1$ a. Then we run the model as in the EISMINT experiment for 25 000 a to reach the steady state. As we also want to compare our scheme with numerical models used in EISMINT, we first perform a model run with 28 nodes. With the same number of grid points as used in the fixed grid models included in EISMINT we are able to obtain a very good estimation for the position of the margin at steady state (commiting an absolute error of only 138.5 m for an exact position $r_l^{\infty} \approx 579.81$ km) without losing accuracy on the ice thickness (see Fig. 3). The estimation of the ice thickness at the ice divide is 3009.5 m compared to 2982.3 ± 26.4 m obtained by 2-D fixed grid models (we exclude 3-D models from our comparison as we only use radial symmetry, see Huybrechts et al., 1996) and compared to 2987 ± 0.01 m obtained by a numerical integration of Eq. (21) that we carried out by using a composite trapezoidal rule.

We also study the convergence of our method towards the reference solution in this case when the number of grid points is increased. We observe that the error for the margin position decreases at an almost quadratic rate $O(n_r^{1.95})$ and the error in the ice thickness at the ice divide at a linear rate $O(n_r^{1.16})$ (results obtained by performing experiments with an initial uniformly spaced grid with $n_r = 20, 28, 40, 60$ and 80 grid points).

4.2 Steady states with non-flat bedrock

The steady state approach of the previous section is still valid for an ice sheet lying on a non-flat bedrock. However, the experiments in such cases are quite limited as we only have the position of the steady margin from Eq. (20). Nevertheless we carry out a few experiments in this context in order to demonstrate that the CMF moving point approach is perfectly suitable for non-flat bedrock.

We consider the following fixed bedrock elevation:

$$b(r) = 2000\,\mathrm{m} - 2000\,\mathrm{m}\left(\frac{r}{300\,\mathrm{km}}\right)^2 + 1000\,\mathrm{m}\left(\frac{r}{300\,\mathrm{km}}\right)^4 - 150\,\mathrm{m}\left(\frac{r}{300\,\mathrm{km}}\right)^6 \tag{24}$$

Figure 5: The reference ice sheet profile ($\varepsilon = 0$) displayed for $t = 100\,\mathrm{a}$, $t = 1000\,\mathrm{a}$, and at $1000\,\mathrm{a}$ intervals thereafter. Rapid changes occur in the state of the sheet at the beginning of the simulation, then the dynamics dramatically slow. The ice thickness at the ice divide decreases at a rate $t^{-1/9}$ and the position of the margin increases at a rate $t^{1/18}$.

following family of similarity solutions

$$h^{(\varepsilon)}(t; r) = \frac{1}{t^{\,(\varepsilon)}} \quad h^{\frac{2n+1}{}}$$

with a grid made up of 100 nodes, uniformly distributed at the initial time. In terms of thickness, errors mostly occur near the ice sheet margin (Fig. 6) as is the case with xed grid methods (see Bueler et al., 2005). However, the position of the ice sheet margin is well estimated, the estimated error being kept under one kilometer (Fig. 7).

Figure 6: The result obtained at nal time t = 20 000a for " = 0 with 100 nodes equally distributed at initial time t = 100 a and a xed time step t = 0:01 a is compared to the reference. A maximum error of 134 m on the ice thickness is obtained at the margin, while the interior of the sheet has errors less than 10 m. The position of the margin is obtained with an error of 880 m.

Figure 7: Evolution of the RMS error and maximum absolute error in the ice thickness, and absolute error in the position of the margin during the run, for the case" = 0 with 100 nodes

Table 2: Rate of convergence of different errors between numerical results obtained for time-dependent solutions at time $t = 20\,000$ a. The different estimated rates of convergence are obtained by performing experiments with $n_r = 10; 20; 40; 60; 80; 100$ and 200 grid points for different configurations of surface mass balance (Eq. 25).

	" = 0	" = 1=8	" = 1=4	" = 3=4
RMS error on h	O			

B A nite di erence algorithm

The moving point method is discretised on a radial line using nite di erences on the grid $\{\hat{r}_i\}$, $i = 1, \dots, n_r$ where

$$0 = \hat{r}_1(t) < \hat{r}_2(t) < \dots < \hat{r}_{n_r - 1}(t) < \hat{r}_{n_r}(t) = r_I(t); \tag{33}$$

The approximation of $h(t; r)$ at $\hat{r}_i$

B.5 Approximate ice thickness

The ice thickness for interior nodes h_i^{k+1} is recovered algebraically at the new time using an order-2 midpoint approximation of Eq. (15), namely,

$$h_i^{k+1} = \frac{{}^{k+1}}{\quad} \frac{{}_{i+1} \quad {}_{i\ 1}}{\hat{r}_{i+1}^{k+1\ 2} \quad \hat{r}_{i\ 1}^{k+1\ 2}} \tag{42}$$

The ice thickness at the ice divide h_1^{k+1} is obtained by using the order-1 upwind scheme.

$$h_1^{k+1} = \frac{{}^{k+1}}{\quad} \frac{{}_{2} \quad {}_{1}}{\hat{r}_{2}^{k+1\ 2} \quad \hat{r}_{1}^{k+1\ 2}} \tag{43}$$

B.6 Behaviour of the approximate ice velocity at the ice margin

As in Sect. 3.4, assuming the topography of the bedrock is at at the vicinity of the margin, the asymptotic form of the radial ice velocity is

$$U = \frac{2}{n+2} A\ ({}_i g)^n\ {}^n(r_l \quad r)^{(2n+1)} \quad {}^n g_l^{2n+1} \tag{44}$$

Hence the leading term in the numerical approximation (Eq. 36) to the ice velocity at the approximation h_l to the ice margin is

$$2$$

R. C. A. Hindmarsh and E. Le Meur. Dynamical processes involved in the retreat of marine ice sheets. J. Glaciol., 47(157):271{282, 2001. doi: 10.3189/172756501781832269.

K. Hutter. Theoretical Glaciology. D. Reidel, Dordrecht, the Netherlands, 1983.

P. Huybrechts, A. J. Payne, and The EISMINT Intercomparison Group. The EISMINT benchmarks for testing ice-sheet models. Ann. Glaciol., 23:1{12, 1996.

T. E. Lee, M. J. Baines, and S. Langdon. A nite di erence moving mesh method based on conservation for moving boundary problems. J. Comput. Appl. Math., 288:1{17, 2015. doi: 10.1016/j.cam.2015.03.032.

G. J. Leysinger Vieli and G. H. Gudmundsson. On estimating length uctuations of glaciers caused by changes in climatic forcing. J. Geophys. Res.-Earth, 109(F01007), 2004. doi: 10.1029/2003JF000027.

D. Partridge. Numerical modelling of glaciers: moving meshes and data assimilation. PhD thesis, University of Reading, Reading, Berks, UK, June 2013. URL http://www.reading.ac.uk/web/FILES/maths/DP_PhDThesis.pdf.

F. Pattyn, L. Perichon, G. Durand, L. Favier, O. Gagliardini, R. C. A. Hindmarsh, T. Zwinger, T. Albrecht, S. Cornford, D. Docquier, J. J. Fürst, D. Goldberg, G. H. Gudmundsson, A. Humbert, M. Hütten, P. Huybrechts, G. Jouvet, T. Kleiner, E. Larour, D. Martin, M. Morlighem, A. J. Payne, D. Pollard, M. Rückamp, O. Rybak, H. Seroussi, M. Thoma, and N. Wilkens. Grounding-line migration in plan-view marine ice-sheet models: results of the ice2sea MISMIP3d intercomparison. J. Glaciol., 59(215):410{422, 2013. doi: 10.3189/2013JoG12J129.

A. J. Payne, P. Huybrechts, A. Abe-Ouchi, R. Calov, J. L. Fastook, R. Greve, S. J. Marshall, I. Marsiat, C. Ritz, L. Tarasov, and M. P. A. Thomassen. Results from the EISMINT model intercomparison: the e ects of thermomechanical coupling. J. Glaciol., 46(153):227{238, 2000. doi: 10.3189/172756500781832891.

G. Scherer and M. J. Baines. Moving mesh nite di erence schemes for the porous medium equation. Mathematics Report Series 1/2012, Department of Mathematics and Statistics, University of Reading, Reading, Berks, UK, 2012. URL https://www.reading.ac.uk/web/FILES/maths/godelareport.pdf.

C. Schoof and R. C. A. Hindmarsh. Thin- lm ows with wall slip: an asymptotic analysis of higher order glacier ow models. Q. J. Mech. Appl. Math., 63(1):73{114, 2010. doi: 10.1093/qjmam/hbp025.

G. G. Stokes. On the Theories of Internal Friction of Fluids in Motion. Transactions of the Cambridge Philosophical Society, 8:287{305, 1845.

A. Vieli and A. J. Payne. Assessing the ability of numerical ice sheet models to simulate grounding line migration. J. Geophys. Res.-Earth, 110(F01003), 2005. doi: 10.1029/2004JF000202.